# Uncertainty Quantification of a Nonlinear Aeroelastic System Using Polynomial Chaos Expansion With Constant Phase Interpolation

**Ajit Desai**[1]
Department of Aerospace Engineering,
IIT Madras,
Chennai 600036, India

**Jeroen A. S. Witteveen**[2]
Center for Turbulence Research,
Stanford University,
Stanford, CA 94305

**Sunetra Sarkar**[3]
Associate Professor
Department of Aerospace Engineering,
IIT Madras,
Chennai 600036, India
e-mail: sunetra.sarkar@gmail.com

*The present study focuses on the uncertainty quantification of an aeroelastic instability system. This is a classical dynamical system often used to model the flow induced oscillation of flexible structures such as turbine blades. It is relevant as a preliminary fluid-structure interaction model, successfully demonstrating the oscillation modes in blade rotor structures in attached flow conditions. The potential flow model used here is also significant because the modern turbine rotors are, in general, regulated in stall and pitch in order to avoid dynamic stall induced vibrations. Geometric nonlinearities are added to this model in order to consider the possibilities of large twisting of the blades. The resulting system shows Hopf and period-doubling bifurcations. Parametric uncertainties have been taken into account in order to consider modeling and measurement inaccuracies. A quadrature based spectral uncertainty tool called polynomial chaos expansion is used to quantify the propagation of uncertainty through the dynamical system of concern. The method is able to capture the bifurcations in the stochastic system with multiple uncertainties quite successfully. However, the periodic response realizations are prone to time degeneracy due to an increasing phase shifting between the realizations. In order to tackle the issue of degeneracy, a corrective algorithm using constant phase interpolation, which was developed earlier by one of the authors, is applied to the present aeroelastic problem. An interpolation of the oscillatory response is done at constant phases instead of constant time and that results in time independent accuracy levels.* [DOI: 10.1115/1.4024794]

## 1 Introduction

Aeroelastic instability remains an important concern for the design of wind turbine rotors, more so with the use of increasingly flexible blades. This increased flexibility brings in complex oscillation modes which could be a potential threat to the safety of the blades. Moreover, it is becoming increasingly recognized that for the design of a complex engineering system, such as a wind turbine, it is crucial to consider the effect of system uncertainties [1]; uncertainties considered in the computational models would enhance the reliability of the design predictions. Uncertainty is an integral part of any system. Uncertainties could arise due to insufficient knowledge of system parameters, modeling assumptions, human error in measurement, or inherent noise present in the system [2]. Traditionally aeroelastic design relies on deterministic models. However, due to the aforementioned reasons and the critical speed being sensitive to the system uncertainties, one should include the input uncertainties in the design in a proper stochastic framework. However, considering the effect of input uncertainties could pose a significant challenge to the designer since the computational framework needed to accommodate the uncertainty quantification analysis could be quite tedious. It is also sometimes necessary to look for the right and most appropriate uncertainty quantification algorithm suitable for various complex design processes.

The most common method used to quantify the effect of uncertainty in a system is the Monte Carlo simulation (MCS). However, it involves generating an ensemble of realizations of the random parameters and repeated deterministic analysis corresponding to each of these realizations. Since the accuracy of the MCS procedure depends on the ensemble size $N$ and the convergence rate is only $O(N^{0.5})$, the MCS can be extremely time consuming and computationally expensive; more so if a large order high fidelity system is involved. Hence, there is a need to look for alternate techniques that are computationally more efficient than the direct MCS procedure. Polynomial chaos expansion (PCE) is such an approach, pioneered by Ghanem and Spanos [3] as a stochastic finite element method in the field of structural mechanics. This is often called a spectral technique since it uses a spectral representation of the uncertainty in terms of orthogonal polynomials. In the original form, is uses Hermite polynomials as the basis along the random dimension and involves Gaussian random variables [4]. A standard Galerkin projection is applied along the random dimensions in order to obtain the governing equations in their weak form. The resulting systems are solved for the coefficients of the random modes [5]. Convergence behavior has been investigated for various Gaussian and non-Gaussian random inputs using Hermite polynomials as compared to other families of orthogonal polynomials from the Askey family [6].

Although the polynomial chaos method was initially generalized to polynomials of the Askey scheme only, the extension to arbitrary random distributions soon followed. By employing the correspondence between the probability density function (PDF) and the weighting function in the orthogonality relation, we can generate optimal expansion polynomials for an arbitrary random

---

distribution. The resulting expansion polynomials need not necessarily come from the Askey scheme. There exist various ways to calculate these optimal expansion polynomials; see, for instance, Refs. [7–9].

The Galerkin projection step modifies the governing equations to a coupled form, which is very complex at times (depending on the uncertainties present and also the nonlinearities in the system) and arriving at them can also be a tedious task. This PCE approach is often referred to as the intrusive approach. For high fidelity and complex systems this could be prohibitively costly. As a result, uncoupled alternatives in the PCE family have been developed. The most important one among the various nonintrusive approaches is the probabilistic collocation method. This chooses some specific optimal points along the random dimension (collocation points) and runs the system at these points. This is similar to the MCS but the number of deterministic runs required is very small. The complete stochastic response can be reproduced using the collocation data and an interpolation polynomial. It is standard practice to use the Gauss quadrature points as the collocation nodes [10,11]. Another noninturusive alternative is the spectral projection method [12]. This approach projects the response against each basis function using inner products and employs the polynomial orthogonality properties to extract each coefficient. Each inner product involves a multidimensional integral over the support range of the weighting function, which can be numerically evaluated using a sampling approach, a numerical quadrature, or a sparse grid [13]. The system has to be run deterministically at specific integration node points, which is similar to the collocation approach. However, the time taken is a very small fraction of the full order MCS, thus making it computationally lucrative. Pettit and his coworkers [14,15] have applied this approach for an aeroelastic model with bending torsion flutter. In a recent study, Chassaing et al. [16] have used a stochastic projection based piecewise polynomial chaos approach in a bending-torsion flutter system subject to supersonic loads. A hard spring nonlinearity was considered in the model. The piecewise spectral approach was able to capture the sharp changes in the stochastic bifurcation behavior. In a separate series of work on aeroelastic instabilities, Poirel and Price [17,18] have studied a nonlinear classical flutter problem with random gusts. They have used a Monte Carlo based approach to follow the stochastic bifurcation behavior.

In our earlier work on an uncertain aeroelastic system, we have used a Gauss–Hermite quadrature scheme to evaluate the chaos coefficient in a one-dimensional approach [19,20]. Since Gaussian random variables and Hermite polynomials were involved, the Gauss–Hermite quadrature gives an optimal converges with minimal nodes. In the present study, we use the approach for a multirandom variable model. This is performed on a multidimensional random domain in which the quadrature locations are the tensor products of the single dimensional quadrature nodes. Additionally, in the present study, parameter variations have been tracked for both single and multiple bifurcations in a series. The performance of the multidimensional PCE in capturing the series of stochastic bifurcations is investigated.

The second aspect of the study is the investigation of the long term degeneracy problem. Generalized polynomial chaos (gPC) has nonuniform convergence and tends to break down for long time integration. The reason is the increased nonlinearity of the response surface with increased time. This is a problem in systems with an oscillatory response in which the response frequency becomes random. As a result, the probability density function (PDF) of the solution evolves as a function of time. The set of orthogonal polynomials associated with the initial distribution will, therefore, not be optimal at later times, thus reducing the efficiency of the method for long-term simulation. This is discussed in Refs. [15,21–25] and is also observed in our flutter periodic solutions. This is, at the moment, an active area of research and several adaptive approaches are being proposed to tackle the problem.

Pettit and Beran [14] have applied a Wiener–Haar expansion to overcome the long time degeneracy problem. Wan and Karniadakis

[25,26] have developed an adaptive multi-element generalized polynomial chaos method (ME-gPC) as a robust scheme to alleviate the problem of long term degeneracy and discontinuity in the random space. The main idea of the ME-gPC is to adaptively decompose the space of random inputs into multiple elements and subsequently employ polynomial chaos expansions at the element level. Lucor and his coworkers [16,27] have applied a similar technique, but a noninturusive multi-element polynomial chaos formulation, to aeroelastic systems in order to predict the stochastic response in the presence of discontinuities in the random space. Millman et al. [22,24] have developed a stochastic projection method based on the Fourier chaos expansion and the noninturusive B-spline stochastic projection in order to capture the sharp discontinuities in the subcritical bifurcation behavior along with the long term periodic behavior. In another approach, Gerritsma et al. [28] have defined new stochastic variables and corresponding orthogonal polynomials are constructed as time progresses. With the new stochastic variables the solution can be represented exactly by linear functions. This allows the method to use very low order polynomial approximations with high accuracies. An algorithm based on constant phase interpolation [20,29,30] was also developed to deal with the long time degeneracy problems. Le Maitre et al. [31] used a similar principle in their work on the PCE with asynchronous time integration. The constant phase interpolation method is described in more detail later in the paper. In the present work, we apply this technique to a two-random variable model and investigate the approach in terms of computational effort and possible applicability to even higher order cases.

We consider a classical aeroelastic model with system nonlinearity and a potential flow model. Although modern flexible rotors can encounter the dynamic stall regime during their operation, the chances of stall induced vibration is minimized by stall and pitch regulation. The idea is to use the classical model to check how the multiparameter PCE works with 2D quadrature in capturing the series of bifurcations and also to investigate the cause and propagation of degeneracy. The second bifurcation point is important because even if the structure survives the onset of oscillation (first bifurcation point), it may encounter a catastrophic situation following the second bifurcation. It is, therefore, crucial to accurately predict both bifurcations in the presence of uncertainty, which is the primary focus area of this study.

In the next section, we discuss the nonlinear aeroelastic model and present the governing equations. In Sec. 3, a brief overview of the PCE approach and the present formulation for a two-random variable quadrature scheme is given. Section 4 discusses the results for two-random variable cases. The long term degeneracy problem and the constant phase algorithm are discussed in Sec. 5. In Sec. 6, this algorithm is applied for the present multirandom variable cases and the last section summarizes the conclusions from the study.

## 2 Nonlinear Aeroelastic System

Figure 1 shows a schematic plot of the two degree-of-freedom pitch-plunge aeroelastic system along with the notations used in the analysis. The aeroelastic equations of motion for the linear
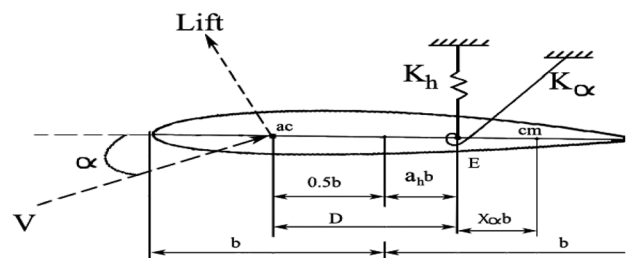


Fig. 1 The schematic of a symmetric airfoil with pitch and plunge degrees-of-freedom

system have been derived by Fung [32]. For nonlinear restoring forces such as with cubic springs in both pitch and plunge, the mathematical formulation is given by Lee et al. [33] in the nondimensional form as follows:

$$\varepsilon'' + x_\alpha \alpha'' + 2\zeta_\varepsilon \frac{\overline{\omega}}{U}\varepsilon' + \left(\frac{\overline{\omega}}{U}\right)^2 (\varepsilon + \beta_\varepsilon \varepsilon^3) = -\frac{1}{\pi\mu}C_L(\tau)$$

$$\frac{x_a}{r_\alpha^2}\varepsilon'' + \alpha'' + 2\frac{\zeta_\alpha}{U}\alpha' + \frac{1}{U^2}(\alpha + \beta_\alpha \alpha^3) = \frac{2}{\pi\mu r_\alpha^2}C_M(\tau) \qquad (1)$$

where $\varepsilon$ denotes the nondimensional displacement of the elastic axis point, $\alpha$ is the pitch angle about the elastic axis. Let us also use $v$ as the wind velocity and $b$ as the half chord. Here, $\tau = vt/b$ is the nondimensional time, $U = v/(b\omega)$ is the nondimensional velocity (also called the reduced velocity), and $\overline{\omega} = \omega_\varepsilon/\omega_\alpha$, $\omega_\varepsilon$, and $\omega_\alpha$ are the natural frequencies of the uncoupled plunging and pitching modes, respectively. In the structural part $\zeta_\alpha$ and $\zeta_\varepsilon$ are the damping ratios in the pitch and plunge, respectively, The mass ratio $\mu$ is defined as $m/\pi\rho v$, with $m$ being the airfoil mass and $\rho$ being the air density. Here, $r_\alpha$ is the radius of gyration about the elastic axis and $x_a$ is the nondimensional distance from the elastic axis to the center of mass. Additionally, $\beta_\alpha$ and $\beta_\varepsilon$ denote the coefficients of the cubic spring in the pitch and plunge, respectively. For the incompressible inviscid flow, Fung [32] gives the expressions for the unsteady lift and pitching moment coefficients $C_L(\tau)$ and $C_M(\tau)$.

Using the Wagner function and introducing a vector of new variables $\{w_1, w_2, w_3, w_4\}$, the original integrodifferential equations for the aeroelastic system given by Eq. (1) are reformulated into a set of first order autonomous differential equations of the form

$$x' = f(\boldsymbol{X}, \text{system parameters}) \qquad (2)$$

where $\boldsymbol{X}$ is an array of eight variables given as

$$\{x_1, x_2, x_3, x_4, x_5, x_6, x_7, x_8\} = \{\alpha, \alpha', \varepsilon, \varepsilon', w_1, w_2, w_3, w_4\}$$

For more details, refer to Lee et al. [33].

## 3 Polynomial Chaos Expansion

The polynomial chaos expansion is a spectral uncertainty quantification tool which offers a means of calculating high-order information such as the mean, variance, and successive moments if the probability density function (PDF) of the input variable is well defined. The original homogeneous polynomial chaos expansion [4] is based on the homogeneous chaos theory of Wiener [34]. This is based on a spectral representation of the uncertainty in terms of orthogonal polynomials. In its original form, it employs Hermite polynomials as a basis from the generalized Askey scheme and Gaussian random variables. Karniadakis et al. [6,35,36] demonstrated that an exponential convergence rate can be achieved in this case for a number of test problems.

In the Galerkin-PCE (also called the intrusive PCE) a standard Galerkin projection is applied along the random dimensions in order to modify the governing equations to a coupled form in terms of the chaos coefficients. Then the resulting deterministic systems are solved using standard techniques to obtain the chaos coefficients [5]. However, these equations are usually more complex and arriving at them is quite often a tedious task for some choices of the uncertain parameters. With an increasing order of expansion, it is required to solve higher order inner products which increases the computational time required to obtain the chaos coefficients and, in some cases, it takes almost the same computational time as the MCS [19].

In order to avoid this, several uncoupled alternatives have been developed based on the observation that the coefficients of the different modes can be obtained by projecting deterministic computations onto the PCE basis. These are collectively called nonintrusive approaches. In the nonintrusive PCE approach, simulations are used as black boxes and the calculation of chaos expansion coefficients for the response is based on a set of simulation response evaluations. The probabilistic collocation method is such a nonintrusive polynomial chaos method in which the problem is collocated at Gauss quadrature points in the probability space [10,11]. The deterministic solutions are performed at these collocation points. The nonintrusive polynomial chaos method proposed by Walters and coworkers [37–39] is based on approximating the polynomial chaos coefficients. A similar approach called nonintrusive spectral projection has been used by Reagan et al. [12,13,40]. Pettit and Beran [14,15] have also used a stochastic projection technique to compute the chaos expansion coefficients in an aeroelastic system. When multiple uncertain parameters are involved, the collocation grids are constructed using tensor products of one-dimensional grids [21,40]. Thus, the number of collocation points and, therefore, the number of required deterministic solutions rapidly increases. As an alternative, sparse grid collocation approaches can be implemented [41–43].

In the present study, a spectral projection based nonintrusive approach [3,44] is used to evaluate the chaos coefficients using the Gauss–Hermite quadrature. Here, the chaos expansions are not substituted in the governing equations; instead, samples of the solutions deterministically evaluated at certain collocation points as in the MCS (we call this step the pseudo-Monte Carlo method) are used to evaluate the coefficients directly using a projection formula. As a result, this approach can utilize the existing deterministic code. Another advantage of this method is that the chaos coefficients are independent of each other.

As per the Cameron–Martin theorem [45], a random process $X(t, \theta)$ (as function of random event $\theta$), which is second order stationary, can be written as

$$X(t,\theta) = \widehat{a}_0 \Psi_0 + \sum_{i_1=1}^{\infty} \widehat{a}_{i_1} \Psi_1\left(\xi_{i_1}(\theta)\right) + \sum_{i_1=1}^{\infty}\sum_{i_2=1}^{i_1} \widehat{a}_{i_1 i_2} \Psi_2\left(\xi_{i_1}(\theta), \xi_{i_2}(\theta)\right)$$
$$+ \sum_{i_1=1}^{\infty}\sum_{i_2=1}^{i_1}\sum_{i_3=1}^{i_2} (\widehat{a}_{i_1 i_2 i_3}) \Psi_3\left(\xi_{i_1}(\theta), \xi_{i_2}(\theta), \xi_{i_3}(\theta)\right) + \cdots \qquad (3)$$

where $\Psi_n(\xi_{i_1}, \xi_{i_2}, \ldots, \xi_{i_n})$ denotes the Hermite polynomial in terms of the $n$-dimensional independent standard Gaussian random variable vector $\boldsymbol{\xi} = (\xi_{i_1}, \xi_{i_2}, \ldots, \xi_{i_n})$ with zero mean and unit variance.

In the original form, the chaos expansion uses Hermite polynomials ($\Psi_n$s); here, $\psi_n$s are the one-dimensional Hermite polynomials as given below

$$\psi_n(\xi) = \xi\psi_{n-1} - (n-1)\psi_{n-2} \qquad (4)$$

One can also use the most appropriate orthogonal polynomials from the generalized Askey scheme for some standard non-Gaussian input uncertainty distributions such as $\gamma$ and $\beta$ [5,6]. For any arbitrary input distribution, a Gram–Schmidt orthogonalization can be employed to generate the orthogonal family of polynomials [8].

Any stochastic process $\alpha(t, \boldsymbol{\xi}(\theta))$, governed by Gaussian random variables $\boldsymbol{\xi}$ ($\boldsymbol{\xi}$ can always be normalized as a standard Gaussian one) can be approximated by the following truncated series

$$\alpha(t, \boldsymbol{\xi}(\theta)) = \sum_{j=0}^{p} \hat{\alpha}_j(t)\Phi_j(\boldsymbol{\xi}(\theta)) \qquad (5)$$

Using the Galerkin projection on Eq. (5) by taking the inner product $\langle ., \Phi_k \rangle$, for $k = 0, 1, \ldots, p$, since the Hermite polynomials are statistically orthogonal, that is, $\langle \Psi_j, \Psi_k \rangle = 0$ for $j \neq k$, the expansion coefficients can directly be evaluated as

$$\widehat{\alpha}_k(t) = \frac{\langle \alpha(t, \xi(\theta)), \Phi_k \rangle}{\langle \Phi_k^2 \rangle} \qquad (6)$$

The denominator in Eq. (6) can be shown to satisfy $\langle \Phi_k^2 \rangle = k!$ for non-normalized Hermite polynomials [14]. Thus, the key step in projecting $\alpha(t, \xi(\theta))$ along the polynomial chaos basis is the evaluation of $\langle \alpha(t, \xi(\theta)), \Phi_j \rangle$. This involves multidimensional integrals which are mainly solved by tensor product quadrature.

In the quadrature based approach, the simplest general technique for approximating a multidimensional integral, as in Eq. (6), is to employ a tensor product of the one-dimensional quadrature rule. There are several choices of quadrature rules which depend upon the weighting function of the integral (the weighting function depends on the choice of the orthogonal polynomials used), e.g., the Gauss–Hermite quadrature, the Gauss–Legendre quadrature, the Gauss–Laguerre quadrature, etc.

Consider a two-random variable case for demonstration. The inner product in the numerator of Eq. (6) is then given by the following integral

$$\langle \alpha(t, \xi(\theta)), \Phi_k \rangle = \int_{-\infty}^{\infty} \int_{-\infty}^{\infty} \alpha(t, \xi_1, \xi_2) \Phi_k \omega(\xi_1, \xi_2) \, \mathrm{d}\xi_1 \mathrm{d}\xi_2 \qquad (7)$$

where the weighting function $\omega(\xi_1, \xi_2)$ is the Gaussian probability density function and is given as follows:

$$\omega(\xi_1, \xi_2) = \left( \frac{1}{\sqrt{(2\pi)^2}} \right) e^{-(1/2)(\xi_1^2 + \xi_2^2)} \qquad (8)$$

A Gauss–Hermite quadrature will be suitable for evaluating the preceding integral as the domain is $(-\infty, \infty)$ and the weight function is a Gaussian PDF. Equation (7) is then rewritten as

$$\langle \alpha(t, \xi(\theta)), \Phi_k \rangle = \frac{1}{2\pi} \sum_{i=1}^{N_0} \sum_{j=1}^{N_0} \left[ \alpha(t, \xi_{1_i}, \xi_{2_j}) \Phi_k(\xi_{1_i}, \xi_{2_j}) \right] W_{1_i} W_{2_j} \qquad (9)$$

where the couples $(\xi_{n_k}, W_k)$ represent the one-dimensional Gauss–Hermite quadrature points and weights. The accuracy of the method is clearly a function of the number of quadrature points $N_0$ [40]. The quadrature points are the zeros of the Hermite polynomials of the chosen order. A number of deterministic runs are performed at the quadrature points, called the pseudo-MCS, which is much lower than the full MCS. The realizations of the system response $\alpha(t, \xi)$ are then used to estimate the deterministic coefficients $\widehat{\alpha}_j(t)$ in Eq. (6) using the Gauss–Hermite quadrature rule as given in Eq. (9). The advantage of quadrature is that it is nonintrusive and the sparse grid approach [42] can be used instead of tensor products to reduce the number of samples in higher dimensions. The accuracy is exponential and it has the flexibility to choose different quadrature rules (Gauss, Clenshaw–Curtis).

## 4 Results for Two-Random Variable Models

The main focus of the present study is quantifying the effect of parametric uncertainties on the bifurcation behavior and the flutter boundary of the nonlinear aeroelastic system. A fourth order variable step Runge–Kutta method is employed for the time integration. The system parameters that are assumed to be uncertain are different combinations of the following parameters $\beta_\alpha$, $\bar{\omega}$, and $\zeta_\alpha$. In the first case, we will consider $\beta_\alpha$ and $\bar{\omega}$ as independent random variables and in the second case, $\beta_\alpha$ and $\zeta_\alpha$ are considered as independent random variables. The rest of the parameters are deterministic and are taken from Ref. [33].
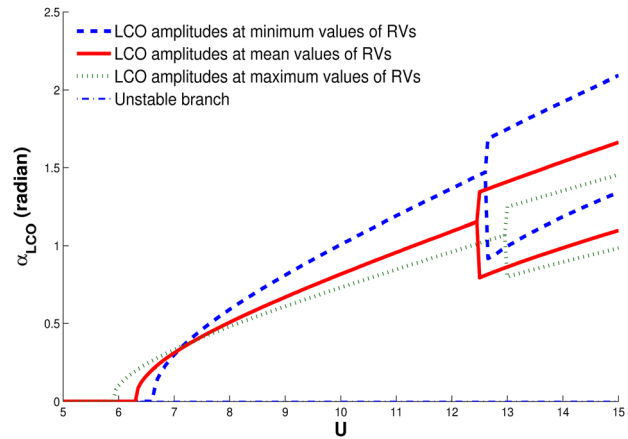
**Fig. 2** Uncertain $\beta_\alpha$ and $\bar{\omega}$: stochastic bifurcation plot

**4.1 Uncertain Structural Nonlinearity and Natural Frequency.** First, we model parametric uncertainties in the cubic spring coefficient ($\beta_\alpha$) and the ratio of the natural frequencies in plunge and pitch ($\bar{\omega}$). These parameters are assumed to be independent Gaussian random variables with a mean of 3.0 and 0.2, respectively; each is assumed to have a coefficient of variation of 0.10. Figure 2 shows the stochastic bifurcation behavior as a function of reduced velocity $U$. Three bifurcation behaviors are plotted. The minimum and maximum branches are obtained by constraining the random domain to ($-4$ to 4) since 99.99% of the realizations of the random variables fall into this domain [46]. The mean branch is obtained by taking the mean values of the input random variables. The first bifurcation (around 6.28 for the mean branch) is a supercritical Hopf bifurcation or a flutter point by which a stable limit cycle oscillation (LCO) emerges and a damped response becomes unstable. The second bifurcation point (around 12.4 for the mean branch) corresponds to a flip bifurcation or a period doubling bifurcation by which the period-1 LCO response becomes unstable and a stable period-2 response emerges. Both the bifurcation points (points of critical $U$) are shifted due to the randomness in the input parameters and the LCO amplitude varies along $U$. However, there are no qualitative changes in the bifurcation behavior due to parametric uncertainties.

In order to show the convergence of the PCE behavior, response PDFs are plotted for various low order PCEs in Fig. 3 at a nondimensional time level of 2000. After the tenth order the convergence is slow. A 25th order expansion is finally chosen to obtain a good match with the MCS, even beyond the chosen time level of 2000. A typical realization time history obtained with the
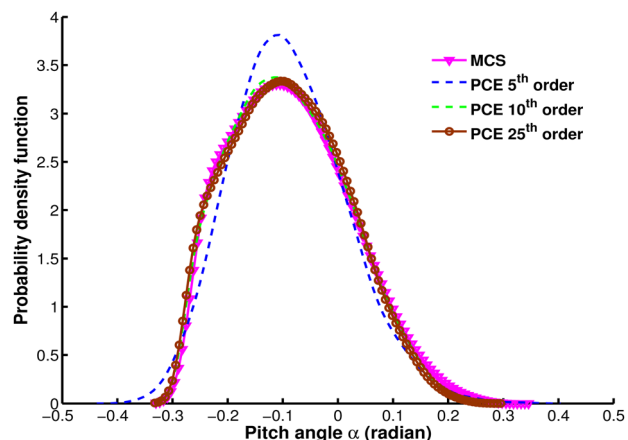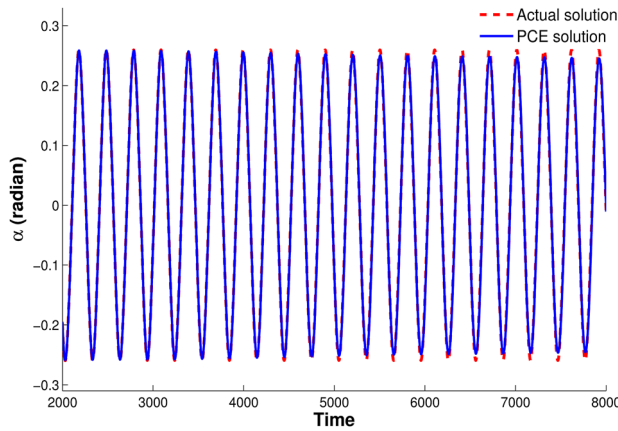


**Fig. 3** Uncertain $\beta_\alpha$ and $\bar{\omega}$: convergence behavior of the PCE at $U = 6.8$ at nondimensional time $t = 2000$

**Fig. 4   Uncertain $\beta_\alpha$ and $\bar{\omega}$: a typical time history with a 25th order PCE at $U = 6.8$**

25th order expansion along with its deterministic counterpart at $U = 6.8$ is shown in Fig. 4. The deterministic solution shown here is the result of numerically solving Eq. (1) for the values of the random parameters corresponding to the PCE realization. The chosen $U$ value is close to the first bifurcation point. To maintain time accuracy for large time we have chosen a 25th order expansion, which is quite high. Convergence of the PCE with an increasing order of PC expansion is given in our earlier work [19,47]. Note that in the present section, we use a 25th order of PC expansion for all the cases. This provides a good long-time accuracy, so that the bifurcation can be studied in detail.

In Fig. 4, the PCE solution matches well with that of the actual solution at the beginning. At around $t = 4000$, the PCE solution starts to degenerate and, as time proceeds, this degeneracy increases. The reason for this mismatch is better understood from Fig. 5, which presents a number of typical realization time histories. Figure 5 shows significant phase shifting, which is more prominent as time proceeds, along with variations in the LCO amplitude. The random variation in the frequency ratio $\bar{\omega}$ affects the frequency of the response, which leads to the phase difference increasing with time. The growing phase difference makes the PDF time dependent and the PCE fails to achieve the same level of accuracy for all time. It is also to be noted that at this $U$, the bifurcation branches are very close to each other, as is also clear from Fig. 2. Possibly both the random variables are canceling the effect of each other around this $U$.

A number of representative PDFs are plotted for the same $U$ in Fig. 6 at different time levels. At $t = 2000$, which is before the degeneracy shows up, there is a good match between the MCS and PCE; a bimodal behavior in the PDF is just seen to be emerg-
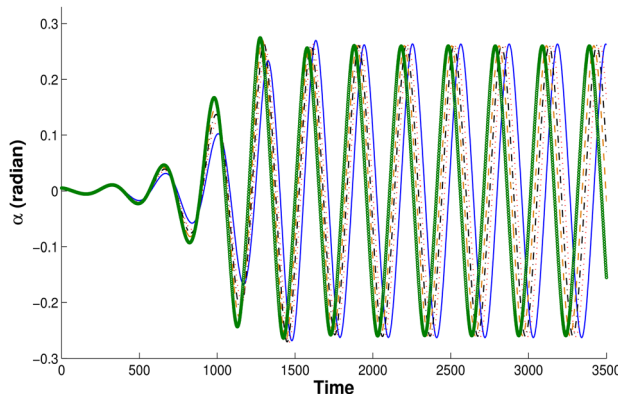


**Fig. 5   Uncertain $\beta_\alpha$ and $\bar{\omega}$: five different realizations of the time history with a 25th order PCE at $U = 6.8$**

ing. This bimodal behavior is due to the phase shifting between the realizations and should become more prominent with time. This is shown in Figs. 6(c) and 6(d), where PDFs are plotted at higher time levels. The bimodal behavior is significant here and the PCE fails to match the reference MCS. It should be noted that with a high order PC expansion (as considered in the present study) an accurate stochastic bifurcation behavior can be predicted since the high order PCE can maintain the accuracy beyond the initial time transients. However, the PDF behavior is accurate only up to a limited time level.

To investigate this long term degeneracy, the time evolution of the chaos expansion coefficients is followed. The corresponding time histories for each $\hat{\alpha}$ are shown in Figs. 7–10. It can be seen that the spectral distribution of the energy in the random dimension shifts to higher chaos modes as time progresses. This is caused by the almost linear response at the beginning and the increasingly oscillatory response surface at later times. Figure 7 shows the first random mode (mean) which contributes mostly at the initial part of the solution and probably contributes very little at higher times. Figure 8(a) shows the next two random modes. The Hermite polynomials used to get these two random modes are constructed using the first two 1-D Hermite polynomials. The maximum amplitude of the chaos coefficients shifts to higher time levels and the contribution of the third mode ($\hat{\alpha}_3$) is comparatively less than the second ($\hat{\alpha}_2$). Figure 8(b) shows the next three random modes plotted together because the 2-D Hermite polynomials used for getting these three random modes are obtained using the first three 1-D Hermite polynomials. Again, in this group of PCE coefficients, the contribution of the first one is dominating and the other two contribute less. Similarly, in Figs. 9 and 10, the groups of higher random modes are plotted. These groups are formed according to the 1-D Hermite polynomials used for their construction. The contribution of the first PCE coefficient in each group is larger compared to the other modes and the energy in the random dimension shifts by each group and not by mode. This shows that the two-random variable case requires an even higher order expansion compared to the single-random variable case, where each random mode contributes to the shifting of the energy to higher PCE modes as time progresses [14]. At time levels above $t = 5000$, the PCE coefficients of the chosen order do not contribute much; hence, the solution starts to degenerate.

Figure 11 shows the LCO amplitude response PDFs as a function of the reduced velocity around the first and second deterministic bifurcation points ($U = 6.285$ and 12.45). Note that these PDFs are obtained before the degeneracy started. As seen from Figs. 11(a) and 11(b), around $U = 6.27$, the PDF is bimodal but shows a larger peak around $\alpha = 0$ as most realizations give a damped response ($\alpha = 0$). At $U = 6.37$, the response PDF is more equally distributed between $\alpha = 0$ and a finite amplitude LCO. As $U$ increases, the number of realizations entering into the LCO increases and, hence, the peak towards the positive $\alpha$ becomes more dominant. Eventually for $U$ above 6.59, single-peak PDFs emerge, indicating a monotonic behavior with all realizations entering the LCO behavior. Thus, the PDFs have clearly gone through a qualitative change, or in other words, a bifurcation. At $U = 12$ (see Figs. 11(c) and 11(d)), single-peak monotonic behavior is observed since all of the response realizations are gathered towards a single value of $\alpha$. From $U = 12.5$ to $U = 12.7$, the response realizations are scattered around more than one value of $\alpha$. Hence, multimodal behavior of the PDFs can be seen. At all of the velocities above $U = 12.7$, the response realizations are scattered around two different $\alpha$ amplitudes. Again, a similar qualitative change, or bifurcation, of the PDFs is observed.

Qualitatively, there is not much difference between the first and the second bifurcation points in terms of the PCE performance. The phase shifting between the realizations is seen to be stronger around the second bifurcation point than the first one and, as a result, the degeneracy rate is faster. The degeneracy experience with the PCE response is quite similar at other velocities and, hence, are not discussed in detail.
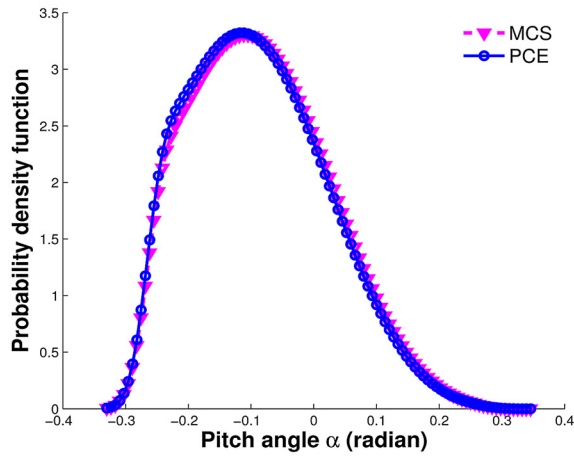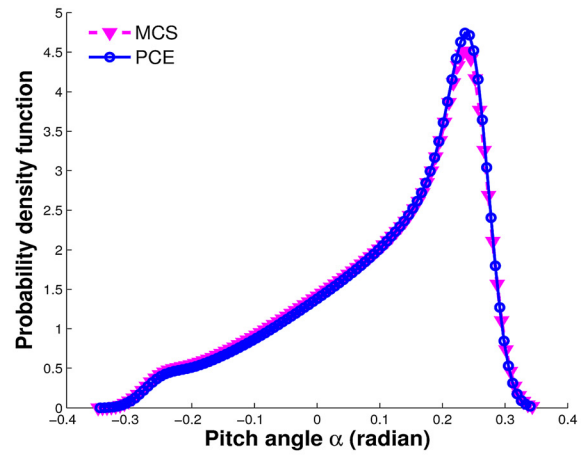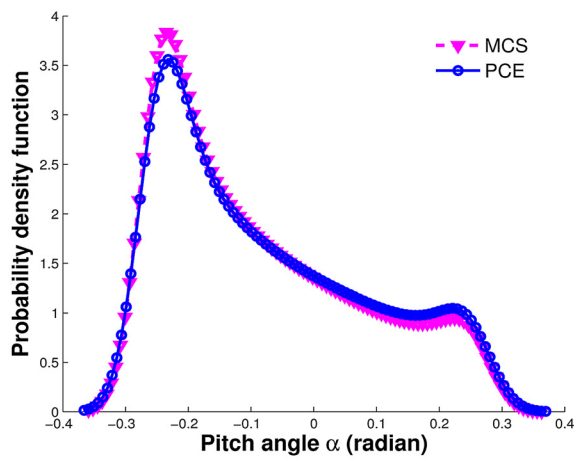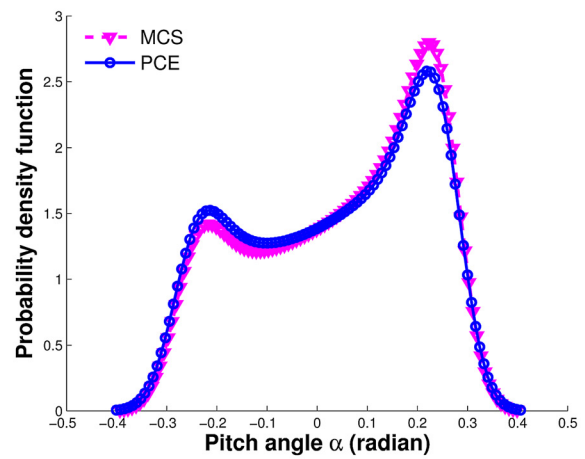
Fig. 6 Uncertain $\beta_\alpha$ and $\bar{\omega}$: comparison of the PDFs obtained by the PCE (25th order) and the MCS with $U = 6.8$ at the nondimensional time (*a*) $t = 2000$, (*b*) $t = 4000$, (*c*) $t = 6000$, and (*d*) $t = 8000$
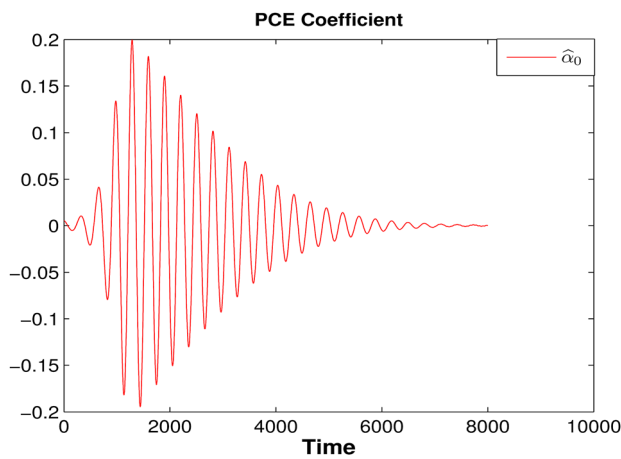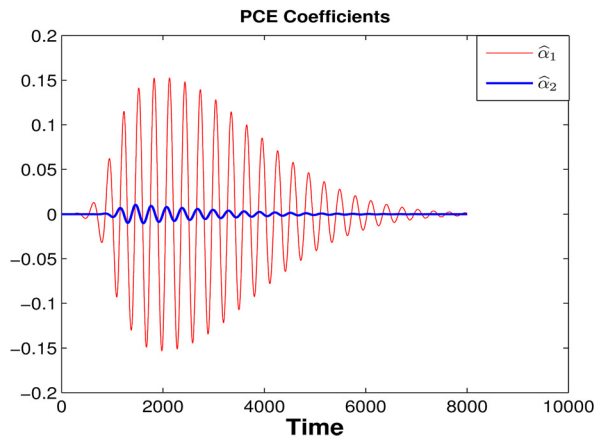


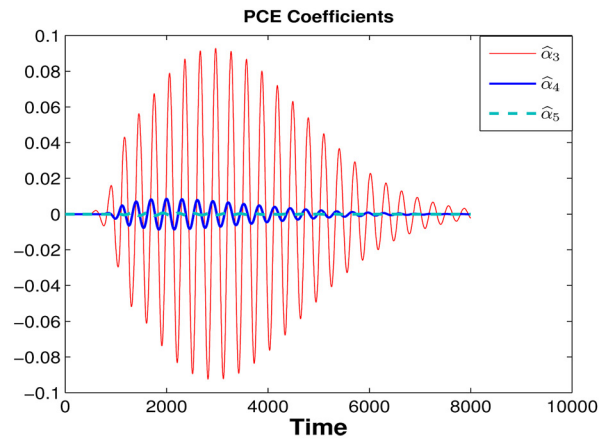Fig. 7 Uncertain $\beta_\alpha$ and $\bar{\omega}$: PCE coefficients at $U = 6.8$

**4.2 Uncertain Structural Nonlinearity and Viscous Damping.** Next, we consider the cubic spring coefficient ($\beta_\alpha$) and viscous damping ratio ($\zeta_\alpha$) as the independent random variables. These parameters are again assumed to be Gaussian random

variables with a mean of 3.0 and 0.1, respectively; each is assumed to have a coefficient of variation of 0.10. The remaining parameters are the same as in the earlier case. Figure 12 shows the stochastic bifurcation plot as a function of the reduced velocity. The minimum and maximum bifurcation branches are plotted by constraining the random domain to ($-4$ to $4$), as in the previous case. The mean branch is plotted at the mean values of the input random variables. Once again, the first bifurcation is a supercritical Hopf bifurcation point, by which a stable LCO emerges and a damped response becomes unstable and the second one is a flip or period doubling bifurcation, by which the period-1 LCO response becomes unstable and a stable period-2 response emerges. Unlike the earlier case, the first critical point remains unaffected and only the second bifurcation point shifts due to the randomness. Fluctuations in structural damping do not affect the oscillation (flutter) onset, unlike the structural natural frequency which had a direct bearing on the critical point. As a result, in this case, there is no shift in the first critical point but only in the oscillation amplitude. In the previous case, both were affected and, as a result, the three branches crossed each other at a velocity beyond the flutter onset (first critical point). The flip bifurcation point is mainly governed by the nonlinearity and behaves in a similar fashion in both cases.
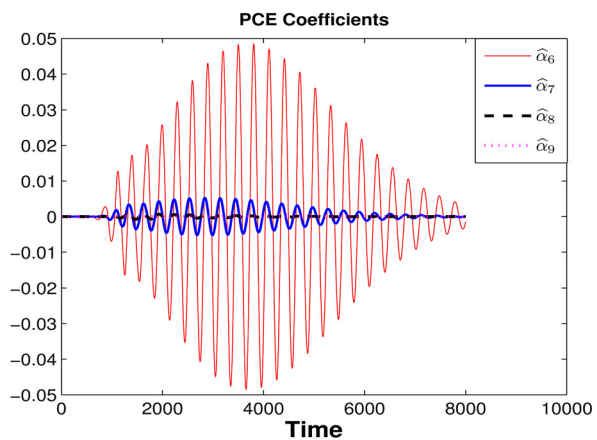
A representative velocity around the first bifurcation point is chosen to discuss the degeneracy behavior. A typical realization
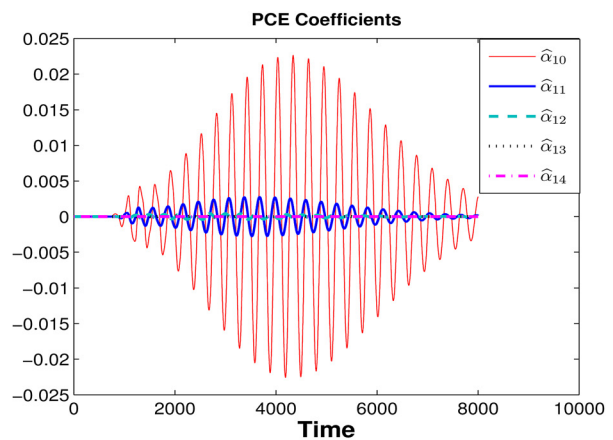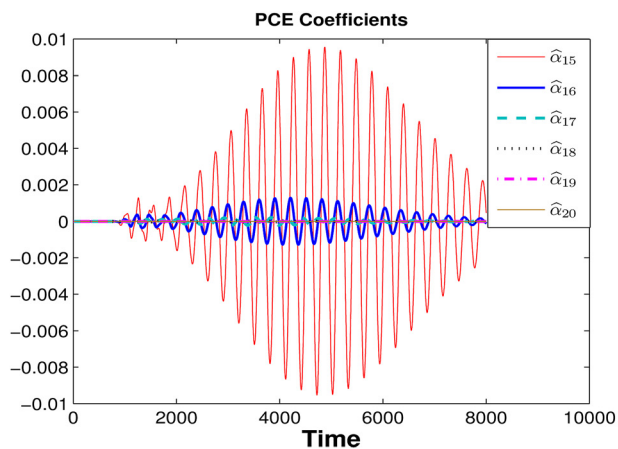
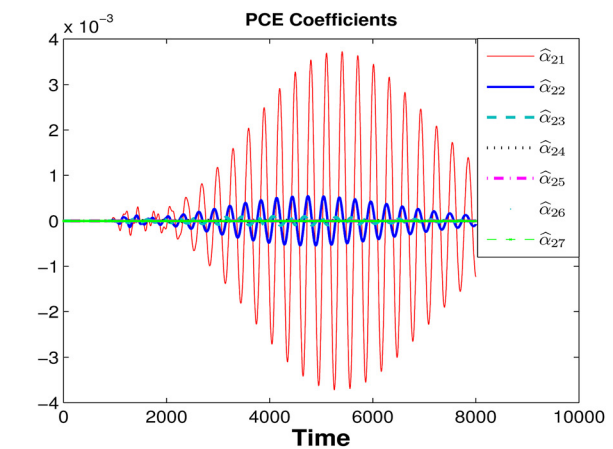**Fig. 8   Uncertain $\beta_\alpha$ and $\bar{\omega}$: PCE coefficients at $U = 6.8$**



**Fig. 9   Uncertain $\beta_\alpha$ and $\bar{\omega}$: PCE coefficients at $U = 6.8$**



**Fig. 10   Uncertain $\beta_\alpha$ and $\bar{\omega}$: PCE coefficients at $U = 6.8$**

time history obtained with the 25th order PCE along with its deterministic counterpart at $U = 6.8$ (taken the same as in the earlier case) is compared in Fig. 13. The match is perfect at the start and, as time proceeds, again, the PCE solution starts degenerating.
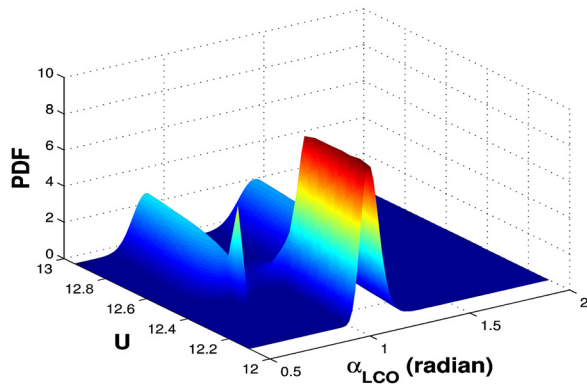
This time degeneracy is much slower and the match is good for a large amount of time. Here we have less phase difference between the response realizations compared to the previous cases. This is presented in Fig. 14, where the time histories for a few typical
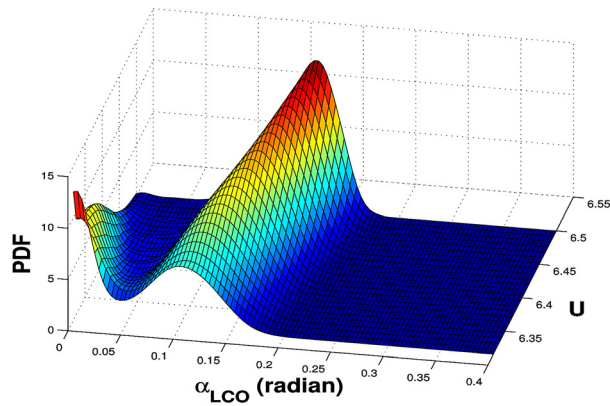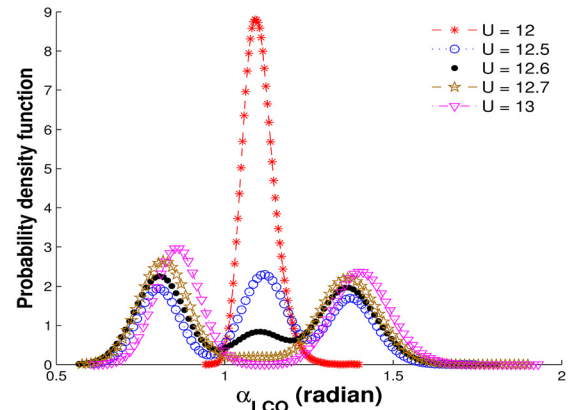
(a) 3D
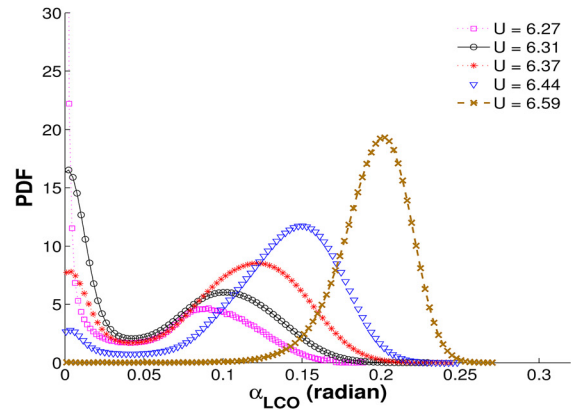


(b) 2D



(c) 3D



(d) 2D

**Fig. 11  Uncertain $\beta_\alpha$ and $\bar{\omega}$: LCO amplitude response PDF as a function of reduced velocity (a),(b) around the first deterministic bifurcation point, and (c),(d) around the second deterministic bifurcation point**
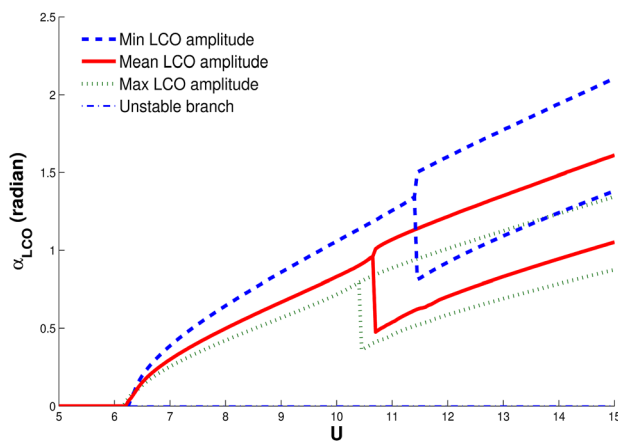


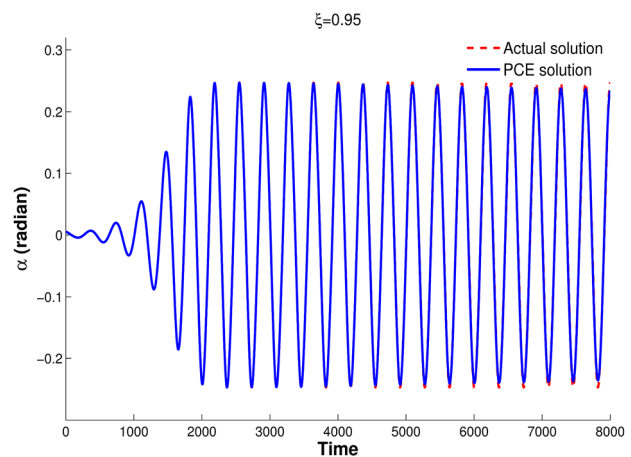**Fig. 12  Uncertain $\beta_\alpha$ and $\zeta_\alpha$: stochastic bifurcation plot**



**Fig. 13  Uncertain $\beta_\alpha$ and $\zeta_\alpha$: a typical time history with the 25th PCE at $U = 6.8$**

samples are plotted. A few representative PDFs at different time levels $t = 4000$, 6000, and 8000 are plotted in Fig. 15 for the same $U$. In Fig. 15(b), the degeneracy has just started and there is a slight mismatch between the PCE and MCS. Figure 15(c) shows PDFs at time $t = 8000$. The bimodal behavior has clearly emerged here and, once again, the PCE shows a slight mismatch with the MCS. Thus, in this case, the effect of degeneracy is much less
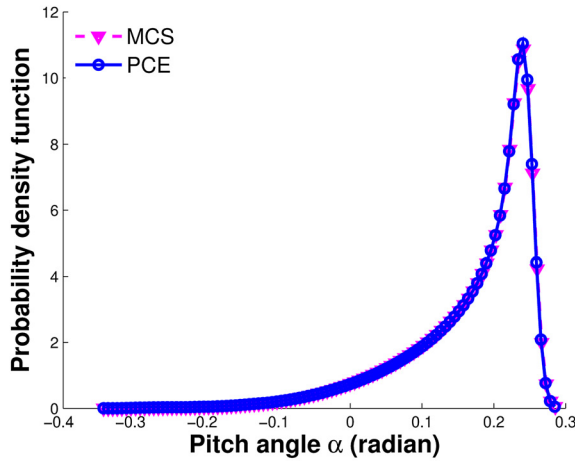
prominent than in the first case because of the smaller impact of $\zeta_\alpha$ on the system frequency. The behavior around the second critical point is also quite similar and is not shown here. The LCO amplitude response PDFs as a function of the reduced velocity are plotted in Fig. 16, around the second bifurcation point. At $U = 10.5$, as all of the realizations are concentrated towards a single value of $\alpha$, single peak monotonic behavior is observed. In the
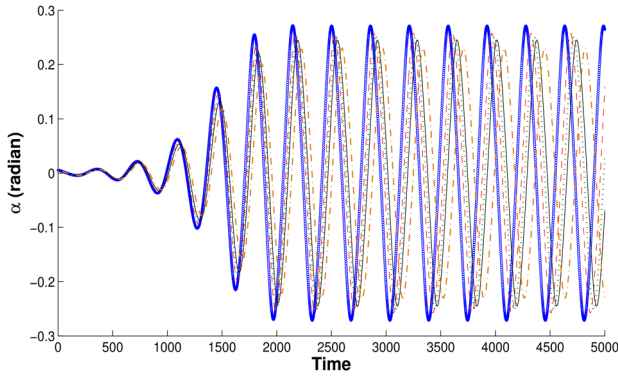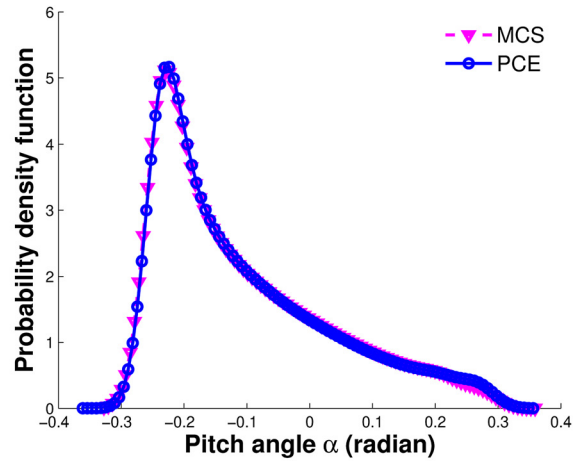
**Fig. 14  Uncertain $\beta_\alpha$ and $\zeta_\alpha$: five different realizations of the time history with a 25th order PCE at $U = 6.8$**
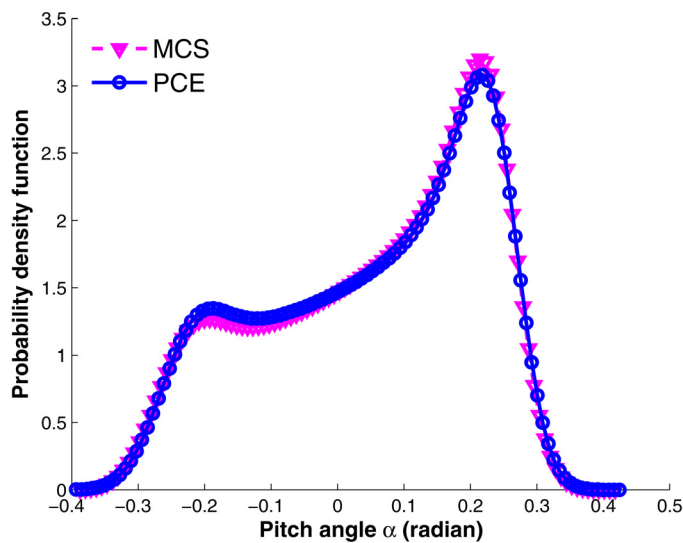
critical range from $U = 10.9$ to $U = 11.5$, the PDFs are bifurcated from single-peak behavior to bimodal behavior due to the occurrence of the higher period LCO after the second bifurcation point. Hence, a bifurcation of PDFs is observed.
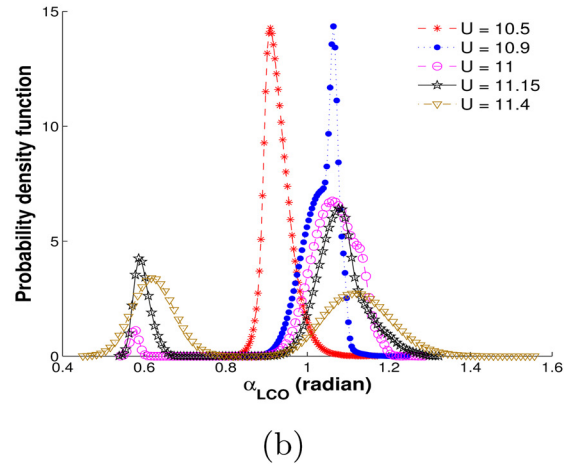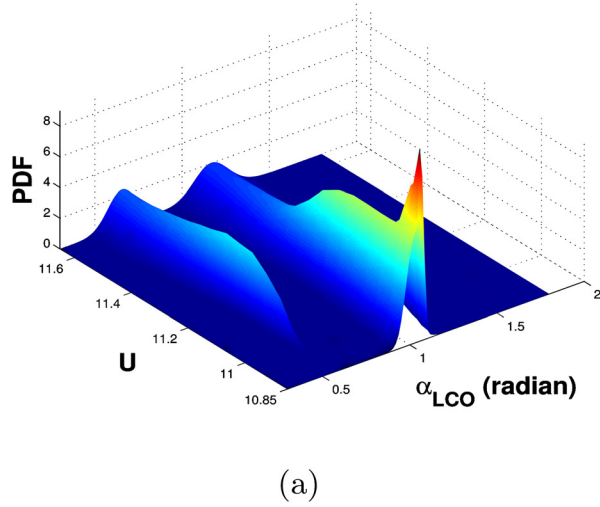
## 5  Long Term Degeneracy

The increasing nonlinearity of the response surface with increasing integration times causes the PCE approach to suffer from a lack of robustness in the modeling of stochastic oscillating systems involving long-term integration. This effect is especially profound in problems with oscillatory solutions in which the frequency of the response is affected by the random parameters. As a countermeasure, one can increase the order of the chaos expansion. However, this can only push the degeneracy to a later time but cannot solve it entirely [23]. In the previous two examples, the effect of degeneracy up to a certain time level is different for different random variable combinations. The higher the phase shifting, the less the time accuracy is for the long time. Below we review the constant phase interpolation algorithm and apply it to the two-random variable cases previously considered.

Polynomial chaos methods usually require a rapidly increasing number of samples with time to maintain a constant accuracy. In Ref. [20], the required number of samples is reduced by applying a one-dimensional collocation rule to a time-independent parameterization for periodic responses. Because of the parameterization, the accuracy of this method is independent of time. The approach



(a)



(b)



(c)

**Fig. 15  Uncertain $\beta_\alpha$ and $\zeta_\alpha$: comparison of the PDFs obtained by the PCE (25th order) and the MCS with $U = 6.8$ at the nondimensional time (a) $t = 4000$, (b) $t = 6000$, and (c) $t = 8000$**

**Fig. 16 Uncertain $\beta_\alpha$ and $\zeta_\alpha$: LCO amplitude response PDF as a function of the reduced velocity about the second bifurcation point (a) 3D, and (b) 2D**

was extended in Ref. [29] to further improve the accuracy and the applicability using an adaptive stochastic finite elements framework with interpolation at constant phase. Here, we combine, for the first time, multidimensional quadrature rules with constant phase interpolation to resolve multiple uncertainties in long-term integration problems with spectral accuracy. The technique is described in detail in the following text.

Performing the uncertainty quantification interpolation of oscillatory samples at constant phase instead of at constant time results in a constant accuracy with a constant number of samples [29]. Assume; therefore, that solving Eq. (1) for the output of interest $u(t, \xi)$ at realizations of the random parameters $\xi_k$ results in oscillatory samples $v_k(t) = u(t, \xi_k)$, of which the phase $v_{\phi_k}(t) = \phi(t, \xi_k)$ is a well-defined monotonically increasing function of time $t$ for $k = 1, .., n_s$, with $n_s$ being the number of samples.

In order to interpolate the samples $\mathbf{v}(t) = \{v_1(t), ..., v_n(t)\}$ at constant phase, first, their phase as a function of time $\mathbf{v}_\phi(t) = \{v_{\phi_1}(t), ..., v_{\phi_n}(t)\}$ is extracted from the deterministic solutions $\mathbf{v}(t)$. The phases $\mathbf{v}_\phi(t)$ are extracted from the samples based on the local extrema of the time series $\mathbf{v}(t)$. A trial and error procedure identifies a cycle of oscillation based on two or more successive local maxima. The selected cycle is accepted if the maximal error of its extrapolation in time with respect to the actual sample is smaller than a threshold value $\bar{\varepsilon}_k$ for at least one additional cycle length. The functions for the phases $\mathbf{v}_\phi(t)$ in the whole time domain $T$ are constructed by identifying all successive cycles of $\mathbf{v}(t)$ and linear extrapolation to $t = 0$ and $t = t_{\max}$ before and after the first and last complete cycle, respectively. The phase is normalized to zero at the start of the first cycle and a user-defined parameter determines whether the sample is assumed to attain a local maximum at $t = 0$. Second, the time series for the phase $\mathbf{v}_\phi(t)$ are used to transform the samples $\mathbf{v}(t)$ into functions of their phase $\hat{\mathbf{v}}(\mathbf{v}_\phi(t))$ according to

$$\hat{v}_k\big(v_{\phi_k}(t)\big) = v_k(t) \tag{10}$$

for $k = 1, ..., n_s$, see Fig. 17. Third, the sampled phases $\mathbf{v}_\phi(t)$ are interpolated to the function $w_\phi(t, \xi)$ using the interpolation method $h$

$$w_\phi(t, \xi) = h\big(\mathbf{v}_\phi(t)\big) \tag{11}$$

as an approximation of the uncertain phase $\phi(t, \xi)$. Finally, the transformed samples $\hat{\mathbf{v}}(\mathbf{v}_\phi(t))$ are interpolated at a constant phase $\varphi \in w_\phi(t, \xi)$ to
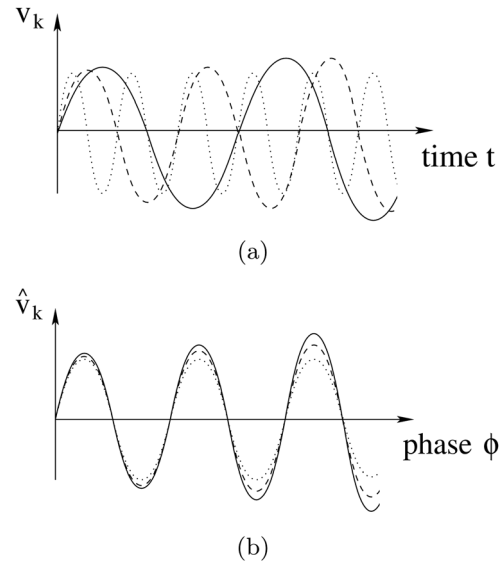
**Fig. 17 Oscillatory samples as a function of time and phase (a) samples $v_k(t)$, and (b) samples $\hat{v}_k(\phi)$**

$$\hat{w}(\varphi, \xi) = h(\hat{\mathbf{v}}(\varphi)) \tag{12}$$

Repeating the latter interpolation for all phases $\varphi \in w_\phi(t, \xi)$ results in the function $\hat{w}(w_\phi(t, \xi), \xi)$. The interpolation $\hat{w}(w_\phi(t, \xi), \xi)$ is then transformed back to an approximation in the time domain $w(t, \xi)$ as follows:

$$w(t, \xi) = \hat{w}\big(w_\phi(t, \xi), \xi\big) \tag{13}$$

The resulting function $w(t, \xi)$ is an approximation of the unknown response surface $u(t, \xi)$ as a function of time $t$ and the random parameters $\xi(\theta)$. This uncertainty quantification formulation for oscillatory responses is proven to achieve a bounded error $\hat{\varepsilon}(\varphi, \xi) = |\hat{w}(\varphi, \xi) - \hat{u}(\varphi, \xi)|$ as a function of phase $\varphi$ for the periodic responses. The error $\varepsilon(t, \xi) = |w(t, \xi) - u(t, \xi)|$ is also bounded in time under certain conditions; see Ref. [48].

## 6 Results for Constant Phase Interpolation

We apply the preceding algorithm to the two-random variable cases considered earlier. To investigate the constant phase
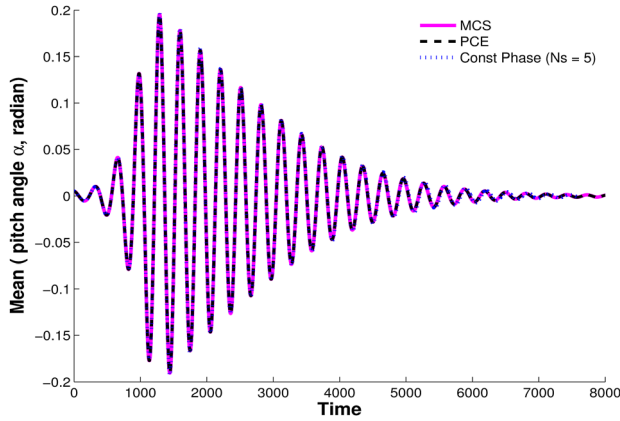
**Fig. 18  Uncertain $\beta_\alpha$ and $\bar{\omega}$: comparison of the time histories of the mean of the pitch angle ($\alpha$) by the MCS, PCE, and constant phase at $U = 6.8$**
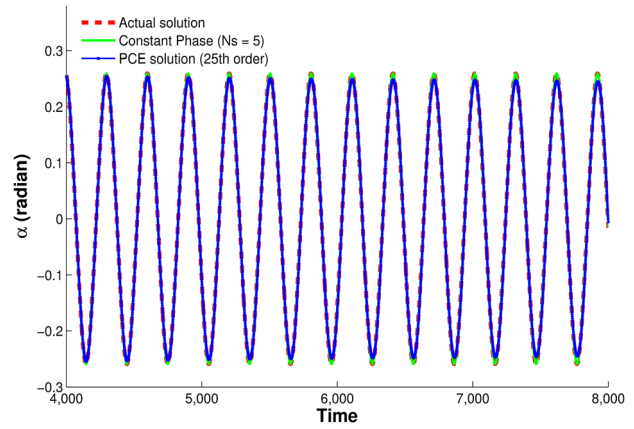


**Fig. 21  Uncertain $\beta_\alpha$ and $\bar{\omega}$: Comparison of the time histories of the pitch angle ($\alpha$) by the MCS, PCE (25th order), and constant phase at $U = 6.8$**
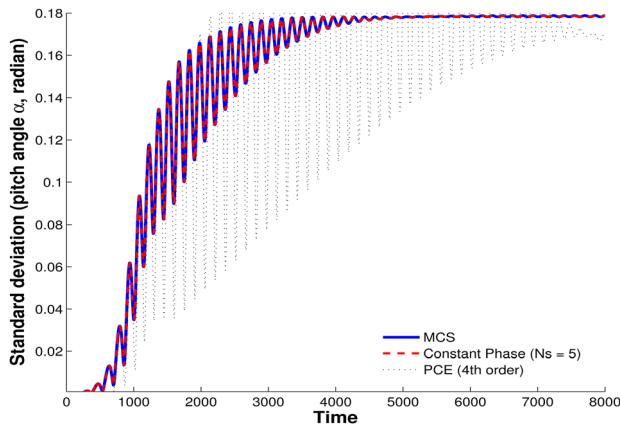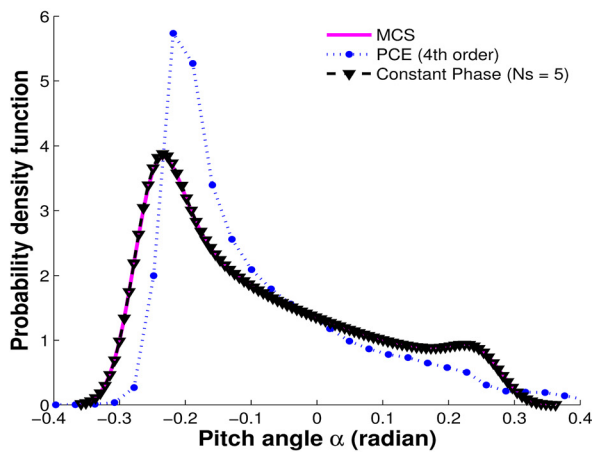
PCE expansion, which is chosen in order to use the same number of deterministic solutions as the constant phase case. This is to highlight the superior accuracy level of the constant phase algorithm with the same number of deterministic solutions.

**6.1  Uncertain Structural Nonlinearity and Natural Frequency.** In the first case of random $\beta_\alpha$ and $\bar{\omega}$, the time degeneracy was quite significant. The constant phase results are shown here for the same cases presented earlier. Figure 18 compares the evolution of the response (pitch angle $\alpha$) mean by a constant phase interpolation algorithm with that of the MCS and PCE near the first critical point $U = 6.8$. The result shows a good match between the constant phase algorithm and the MCS. The mean response is equal to the zeroth order term in the PCE expansion. The time evolution plots for different chaos coefficients showed that the mean is significant at small time levels and decreases to zero at large time levels. Thus, the time degeneracy effect on the mean is insignificant. The standard deviation results by the constant phase algorithm gives a close match to that of the MCS in Fig. 19. These results have also been compared with a fourth order PCE which, quite expectedly, is inaccurate. A fourth order PCE would require a minimum of five quadrature point runs which is equivalent to a five-sample constant phase. Although the number of deterministic runs are the same, the constant phase is able to show an excellent match with that of the reference MCS, whereas the PCE is grossly



**Fig. 19  Uncertain $\beta_\alpha$ and $\bar{\omega}$: comparison of the time histories of the standard deviation of the pitch angle ($\alpha$) by the MCS, PCE, and constant phase at $U = 6.8$**
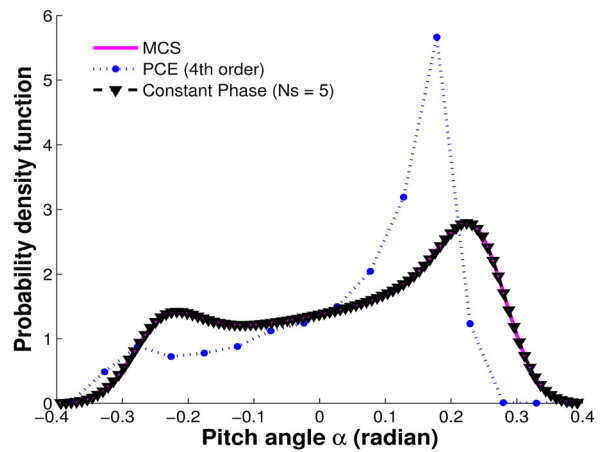
algorithm in these cases, in most situations the number of sampling nodes is kept at five with a piecewise linear interpolation from the nodes to 1000 random interpolation points. In this section, the PCE results are also plotted along with the order of the



(a)



(b)

**Fig. 20  Uncertain $\beta_\alpha$ and $\bar{\omega}$: comparison of the response PDF by the MCS, PCE, and constant phase for $U = 6.8$ at time level (*a*) 6000, and (*b*) 8000**
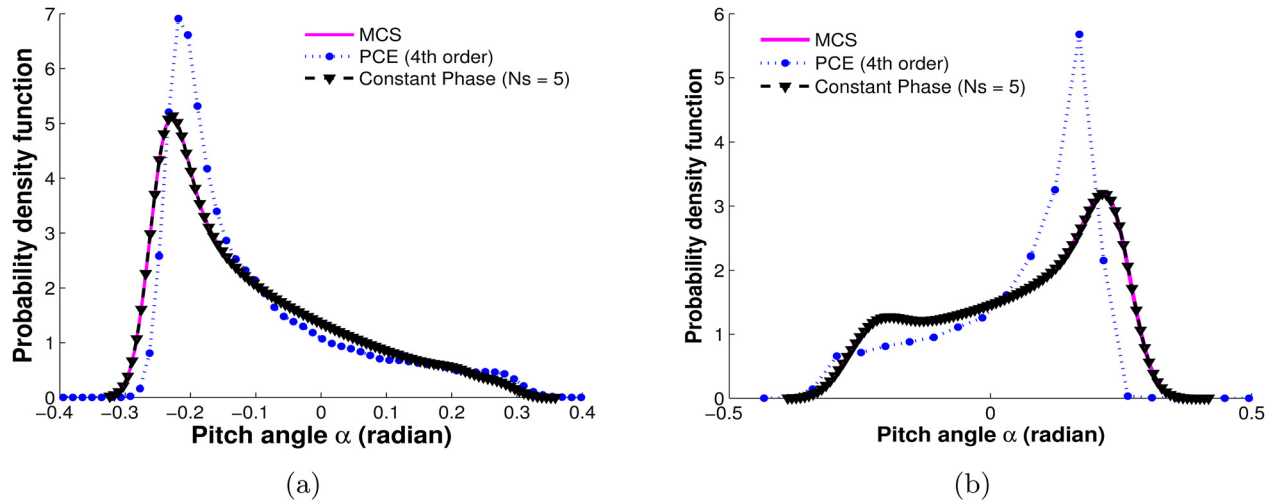
**Fig. 22** Uncertain $\beta_\alpha$ and $\zeta_\alpha$: comparison of the PDFs obtained by the MCS, PCE, and constant phase with five samples, with $U = 6.8$ at the nondimensional time (*a*) $t = 6000$, and (*b*) $t = 8000$

inadequate. In the subsequent analysis, in each case, we will present the constant phase results along with its equivalent order PCE to highlight the advantage of the constant phase algorithm.

In Sec. 4, the PDFs were seen to differ from that of the MCS with increasing time levels. The PDFs at time levels 6000 and 8000 are plotted in Fig. 20 for $U = 6.8$. The effect of time degeneracy was quite prominent for the PCE at these levels and the PDFs at these time levels showed a significant mismatch with the MCS in Fig. 6. On the contrary, with the constant phase algorithm, there is no effect of time degeneracy on the good match with the MCS results, even for the low number of five samples. A comparison of a typical time history is presented in Fig. 21. A full order (25th order) PCE is used here for comparison (as in Sec. 4) to mark the absence of degeneracy, unlike the earlier results.

**6.2 Uncertain Structural Nonlinearity and Viscous Damping.** Once again, the constant phase results are in good agreement with the MCS. The time evolution of the mean and standard deviation match very well with that of the MCS (not shown here) for all times. The response PDF at two representative time levels are shown in Fig. 22 around the first critical point, as was done in Sec. 4. In this case, there has been lesser phase shifting between the response realizations compared to the previous case. The PDFs plotted by using a 5-sample constant phase approach show a very good match with that of the MCS and is an improvement over the PCE predictions of Fig. 15.

The constant phase algorithm uses only a few deterministic runs compared to the 4000 runs of the reference MCS. However, the postprocessing part involving the interpolation requires considerably more time. Hence, for the present low order system, the overall computational effort becomes comparable. However, the present study is only a preliminary step in applying the algorithm eventually to a large order high-fidelity system in which minimizing the number of deterministic solutions is crucial. These results demonstrate that the novel multidimensional PCE with constant phase interpolation is also able to match the MCS results after long time integration for multivariant stochastic inputs. This leads to a significantly more accurate solution than the standard PCE with the same number of samples, especially for the standard deviation and the PDFs.

## 7 Conclusions

In the present study, we have performed a Gauss–Hermite quadrature based polynomial chaos expansion for two-random variable cases. The Gauss–Hermite quadrature ensures that a minimal number of deterministic runs are used as Gaussian probability density

functions (PDFs) and Hermite polynomials are involved. For the nonlinear aeroelastic system considered here, the bifurcation behavior has been investigated. The system is damped below the first critical point and is higher periodic oscillatory beyond the second critical point. A supercritical Hopf bifurcation (flutter) gives way to a period doubling bifurcation and no further bifurcations were seen in the chosen range of velocity. The evolution of the response PDF near these critical points show qualitative changes in their behavior. Tracking the changes in the response PDF and identifying the stochastic onset of the periodic response is, in general, important from a fatigue point of view. The PDFs are estimated after the initial time transients die down. However, it is also observed that the PDFs become increasingly degenerate with time. This behavior is well documented in the literature and is commonly referred to as a time degeneracy problem of uncertain oscillatory response. This is attributed to the increasing phase shifting of the realizations with time. The uncertain input parameters considered in the present problem also lead to a similar phase shifting of the realizations and, as a result, the time accuracy of the polynomial chaos scheme is lost. The extent of the degeneracy is seen to be different for different input uncertainties. To remedy this situation an earlier developed algorithm, called the constant phase interpolation, has been applied here for the present two-random variable cases. This technique significantly improves the time accuracy of the PDFs with a minimal number of deterministic solutions and, thus, also maintains the computational advantage of a nonintrusive scheme. However, it is expected that the number of required samples in the algorithm would increase if the degeneracy becomes severe and a larger number of deterministic solutions would be required. Even then, the total number of deterministic runs are significantly lower than the quadrature-based algorithm. The postprocessing step, however, would require some extra computational effort. Overall, this algorithm shows promise to be applicable to a higher number of random parameters.

## References

[1] Soize, C., Capiez-Lernout, E., Durand, J.-F., Fernandez, C., and Gagliardini, L., 2008, "Probabilistic Model Identification of Uncertainties in Computational Models for Dynamical Systems and Experimental Validation," Comput. Methods Appl. Mech. Eng., **198**, pp. 150–163.
[2] Hamel, J. M., and Azarm, S., 2011, "Reducible Uncertain Interval Design by Kriging Metamodel Assisted Multi-Objective Optimization," ASME J. Mech. Des., **133**, p. 011002.
[3] Ghanem, R., G., and Spanos, P. D., 1991, *Stochastic Finite Elements: A Spectral Approach*, Springer-Verlag, New York.
[4] Wiener, N., 1938, "The Homogeneous Chaos," Am. J. Math., **60**, pp. 897–936.
[5] Xiu, D., and Karniadakis, G. E., 2003, "Modeling Uncertainty in Flow Simulations Via Generalized Polynomial Chaos," J. Comput. Phys., **187**, pp. 137–167.

[6] Xiu, D., and Karniadakis, G. E., 2002, "The Wiener–Askey Polynomial Chaos for Stochastic Differential Equations," SIAM J. Sci. Comput. (USA), **24**(2), pp. 619–644.

[7] Soize, C., and Ghanem, R., 2004, "Physical Systems With Random Uncertainties: Chaos Representations With Arbitrary Probability Measure," SIAM J. Sci. Comput. (USA), **26**, pp. 395–410.

[8] Witteveen, J. A. S., Sarkar, S., and Bijl, H., 2007, "Modeling Physical Uncertainties in Dynamic Stall Induced Fluid-Structure Interaction of Turbine Blades Using Arbitrary Polynomial Chaos," Comput. Struct., **85**, pp. 866–878.

[9] Wan, X., and Karniadakis, G. E., 2006, "Multi-Element Generalized Polynomial Chaos for Arbitrary Probability Measures," SIAM J. Sci. Comput. (USA), **28**, pp. 901–928.

[10] Babuska, I. M., Nobile, F., and Tempone, R., 2007, "A Stochastic Collocation Method for Elliptic Partial Differential Equations With Random Input Data," SIAM (Soc. Ind. Appl. Math.) J. Numer. Anal., **45**(3), pp. 1005–1034.

[11] Loeven, G. J. A., Witteveen, J. A. S., and Bijl, H., 2007, "Probabilistic Collocation: An Efficient Non-Intrusive Approach for Arbitrarily Distributed Parametric Uncertainties," 45th AIAA Aerospace Sciences Meeting and Exhibit, Reno, NV, January 8–11, AIAA Paper No. 2007-317.

[12] Reagan, M. T., Najm, H. N., Ghanem, R. G., and Knio, O. M., 2003, "Uncertainty Quantification in Reacting-Flow Simulations Through Non-Intrusive Spectral Projection," Combust. Flame, **132**, pp. 545–555.

[13] Le Maitre, O. P., Reagan, M. T., Najm, H. N., Ghanem, R. G., and Knio, O. M., 2002, "A Stochastic Projection Method for Fluid Flow: II. Random Process," J. Comput. Phys., **181**, pp. 9–44.

[14] Pettit, C. L., and Beran, P. S., 2006, "Spectral and Multi-Resolution Wiener Expansions of Oscillatory Stochastic Process," J. Sound Vib., **294**, pp. 752–779.

[15] Pettit, C. L., and Beran, P. S., 2004, "Polynomial Chaos Expansion Applied to Airfoil Limit Cycle Oscillations," 45th AIAA/ASME/ASCE/AHS/ASC Structures, Structural Dynamics and Materials Conference, Palm Springs, CA, April 19–22, AIAA Paper No. 2004-1691.

[16] Chassaing, J.-C., Lucor, D., and Trégon J., 2012, "Stochastic Nonlinear Aeroelastic Analysis of a Supersonic Lifting Surface Using an Adaptive Spectral Method," J. Sound Vib., **331**, pp. 394–411.

[17] Poirel, D., and Price, S. J., 2007 "Bifurcation Characteristics of a Two-Dimensional Structurally Nonlinear Airfoil in Turbulent Flow," Nonlinear Dyn., **48**(4), pp. 423–435.

[18] Poirel, D., and Price, S. J., 2003, "Response Probability Structure of a Structurally Nonlinear Fluttering Airfoil in Turbulent Flow," Probab. Eng. Mech., **18**, pp. 185–202.

[19] Desai, A., and Sarkar, S., 2010, "Analysis of a Nonlinear Aeroelastic System With Parametric Uncertainties Using Polynomial Chaos Expansion," Math. Probl. Eng., **2010**, p. 379472.

[20] Witteveen, J. A. S., Loeven, G. J. A., Sarkar, S., and Bijl, H., 2008, "Probabilistic Collocation for Period-1 Limit Cycle Oscillations," J. Sound Vib., **311**, pp. 421–439.

[21] Ghisu, T., Parks, G. T., Jarrett, P. M., and Clarkson, P. J., 2010, "Adaptive Polynomial Chaos for Gas Turbine Compression Systems Performance Analysis," AIAA J., **48**(6), pp. 1156–1170.

[22] Millman, D. R., King, P. I., Raymond, C. M., Beran, P. S., and Chilton, L. K., 2006, "Uncertainty Quantification With a B-Spline Stochastic Projection," AIAA J., **44**, pp. 1845–1853.

[23] Wan, X., and Karniadakis, G. E., 2006, "Long-Term Behavior of Polynomial Chaos in Stochastic Flow Simulations," Comput. Methods Appl. Mech. Eng., **195**, pp. 5582–5596.

[24] Millman, D. R., King, P. I., Raymond, C. M., Beran, P. S., and Chilton, L. K., 2005, "Estimating the Probability of Failure of a Nonlinear Aeroelastic System," J. Aircr., **43**(1), pp. 504–516.

[25] Wan, X., and Karniadakis, G. E., 2005, "An Adaptive Multi-Element Generalized Polynomial Chaos Method for Stochastic Differential Equations," J. Comput. Phys., **209**, pp. 617–642.

[26] Wan, X., and Karniadakis, G. E., 2006, "Beyond Wiener–Askey Expansions: Handling Arbitrary PDFs: An Adaptive Multi-Element Generalized Polynomial Chaos Method for Stochastic Differential Equations," J. Sci. Comput., **27**, pp. 455–464.

[27] Meitour, J. L., Lucor, D., and Chassaing, J. C., 2010, "Prediction of Stochastic Limit Cycle Oscillations Using an Adaptive Polynomial Chaos Method," ASD J., **2**, pp. 3–22.

[28] Gerritsma, M., van der Steen, J. B., Vos, P., and Karniadakis, G., 2010, "Time-Dependent Generalized Polynomial Chaos," J. Comput. Phys., **229**, pp. 8333–8363.

[29] Witteveen, J. A. S., and Bijl, H., 2008, "An Alternative Unsteady Adaptive Stochastic Finite Elements Formulation Based on Interpolation at Constant Phase," Comput. Methods Appl. Mech. Eng., **198**, pp. 578–591.

[30] Witteveen, J. A. S., and Bijl, H., 2009, "Effect of Randomness on Multi-Frequency Aeroelastic Responses Resolved by Unsteady Adaptive Stochastic Finite Elements," J. Comput. Phys., **228**, pp. 7025–7045.

[31] Le Maître, O. P., Mathelin, L., Knio, O. M., and Hussaini, M. Y., 2010, "Asynchronous Time Integration for Polynomial Chaos Expansion of Uncertain Periodic Dynamics," Discrete Contin. Dyn. Syst., **28**, pp. 199–226.

[32] Fung, Y. C., 1955, *An Introduction to the Theory of Aeroelasticity*, John Wiley and Sons, New York.

[33] Lee, B., Jiang, L., and Wong, Y., 1998, "Flutter of an Airfoil With a Cubic Nonlinear Restoring Force," 39th AIAA/ASME/ASCE/AHS/ASC Structures, Structural Dynamics, and Materials Conference and Exhibit, Long Beach, CA, April 20–23, AIAA Paper No. 98-1725.

[34] Wiener, N., 1958, *Nonlinear Problems in Random Theory*, MIT Technology Press and John Wiley and Sons, New York.

[35] Lucor, D., Su, C.-H., and Karniadakis, G. E., 2004, "Generalized Polynomial Chaos and Random Oscillators," Int. J. Numer. Methods Eng., **60**, pp. 571–596.

[36] Lucor, D., and Karniadakis, G. E., 2004, "Adaptive Generalized Polynomial Chaos for Nonlinear Random Oscillators," SIAM J. Sci. Comput. (USA), **26**(2), pp. 720–735.

[37] Hosder, S., Walters, R. W., and Perez, R., 2006, "A Non-Intrusive Polynomial Chaos Method for Uncertainty Propagation in CFD Simulations," 44th AIAA Aerospace Sciences Meeting and Exhibit, Reno, NV, January 9–12, AIAA Paper No. 2006-891.

[38] Walters, R., W., 2003, "Towards Stochastic Fluid Mechanics Via Polynomial Chaos," 41st AIAA Aerospace Sciences Meeting and Exhibit, Reno, NV, January 6–9, AIAA Paper No. 2003-0413.

[39] Hosder, S., Walters, R. W., and Balch, M., 2008, "Efficient Uncertainty Quantification Applied to the Aeroelastic Analysis of a Transonic Wing," 46th AIAA Aerospace Sciences Meeting and Exhibit, Reno, NV, January 7–10, AIAA Paper No. 2008-729.

[40] Le Maître, O. P., Knio, O. M., Najm, H. N., and Ghanem, R. G., 2001, "A Stochastic Projection Method for Fluid Flow: I. Basic Formulation," J. Comput. Phys., **181**(2), pp. 481–511.

[41] Ganappathysubramanian, B., and Zabaras, N., 2007, "Sparse Grid Collocation Schemes for Stochastic Natural Convection Problems," J. Comput. Phys., **225**, pp. 652–685.

[42] Gerstner, T., and Griebel, M., 1998, "Numerical Integration Using Sparse Grids," Numer. Algorithms, **18**, pp. 209–232.

[43] Xiu, D. B., and Hesthaven, J. S., 2005, "High-Order Collocation Methods for Differential Equations With Random Inputs," SIAM J. Sci. Comput. (USA), **27**, pp. 1118–1139.

[44] Millman, D. R., King, P. I., and Beran, P. S., 2003, "A Stochastic Approach for Predicting Bifurcation of a Pitch and Plunge Airfoil," 21st AIAA Applied Aerodynamics Conference, Orlando, FL, June 23–26, AIAA Paper No. 2003-3515.

[45] Cameron, R. H., and Martin, W. T., 1947, "The Orthogonal Development of Nonlinear Functionals in Series of Fourier–Hermite Functionals," Ann. Math., **48**, pp. 385–392.

[46] Millman, D. R., 2004, "Quantifying Initial Conditions and Parametric Uncertainties in a Nonlinear Aeroelastic System With an Efficient Stochastic Algorithm," Ph.D. thesis, Air Force Institute of Technology, Wright-Patterson Air Force Base, OH.

[47] Desai, A., and Sarkar, S., 2010, "Uncertainty Quantification and Bifurcation Behavior of an Aeroelastic System," ASME 7th International Symposium on Fluid-Structure Interations, Flow-Sound Interactions, and Flow-Induced Vibration and Noise, Montreal, Canada, August 1–5, ASME Paper No. FEDSM-ICNMM2010-30050.

[48] Witteveen, J. A. S., and Bijl, H., 2009, "A TVD Uncertainty Quantification Method With Bounded Error Applied to Transonic Airfoil Flutter," Comm. Comp. Phys., **6**, pp. 406–432.